THE ASTRONOMICAL JOURNAL VOLUME 113, NUMBER 4 APRIL 1997

A *ROSAT* PSPC STUDY OF NGC 55

ERIC M. SCHLEGEL,[1,2] PAUL BARRETT,[1] AND KULINDER PAL SINGH[3]
Electronic mail: eschlegel@cfa.harvard.edu, barrett@compass.gsfc.nasa.gov, singh@tifrvax.tifr.res.in

Received 1996 July 17; revised 1996 December 23

ABSTRACT

The Position Sensitive Proportional Counter onboard *ROSAT* imaged the spiral galaxy NGC 55 in X-rays for 18.9 ksec. Twenty-two point-like X-ray sources are detected covering the PSPC field-of-view, of which 7 sources are candidate members of NGC 55. The spectra of the brightest sources that are nearest to NGC 55 are consistent either with a heavily absorbed source or a foreground star. The absorbed sources are very likely members of NGC 55. None of the brightest sources appear to be variable in a periodic fashion. Weak diffuse emission is detected in the plane of the galaxy, but only in the energy bands above ~ 0.5 keV. This emission is either the tail of a hot component of the ISM or the emission of unresolved point sources. We argue that the emission is a hot ISM component. A hot plume, visible in the 0.75 keV band, appears to align with an H I plume detected in a VLA total H I map. The cool H I gas appears to surround the hot gas, so the structure represents a chimney. © *1997 American Astronomical Society.* [S0004-6256(97)01904-3]

1. INTRODUCTION

The study of X-ray emission in external galaxies is very important for understanding the evolution of different populations of X-ray sources and the hot phase of the interstellar medium. The resolution of point sources and the detection of diffuse X-ray emission, however, had been possible in just a few of the galaxies observed with the *Einstein Observatory*, most of which were either in the Local Group or were large, nearby galaxies (viz., LMC, SMC, NGC 253, M31, M33, M81, M82, and M83) (Fabbiano 1989). Nevertheless, these early results provided a great impetus to the study of the X-ray emission of galaxies. The *ROSAT* PSPC, with its higher sensitivity and lower internal background, can extend the study of galaxies to a larger sample. Studies with *ROSAT* have already indicated that diffuse emission is perhaps ubiquitous in spiral galaxies of all types. Here, we present the detection of discrete X-ray sources and extended diffuse X-ray emission in a nearby spiral galaxy, NGC 55.

NGC 55 is classified as a loosely-wound barred spiral (type: SBS9) in the 3rd Revised Catalog of Galaxies (deVaucouleurs *et al.* 1991). It is a member of the Sculptor group which lies at a distance of ~ 1–2 Mpc (Tully 1988; Liller & Alcaino 1983). For this paper, we adopt the distance of 1.6 Mpc as determined by Pritchett *et al.* (1987). NGC 55 is seen nearly edge-on with an inclination of $\sim 80°$ (Hummel *et al.* 1986). The relative proximity of NGC 55 makes it a good candidate for the detection of an X-ray halo, as it is at least a factor of 5 closer than NGC 891 (~ 10 Mpc, Bregman & Pildis 1994) and NGC 4631 (~ 7 Mpc, Wang *et al.* 1995), both of which show diffuse galactic emission. The high inclination introduces considerable source confusion because the galaxy is seen in projection. Our attention was drawn to NGC 55 by the detection of a very soft source that lies near the galaxy. The very soft source was obtained from a study of the entire data base of pointed observations of *ROSAT* (Singh *et al.* 1995). We describe here the results of our study of NGC 55 and the surrounding *ROSAT* field.

This paper is organized as follows. Section 2 describes the observation and the data set. Section 3 presents the analysis and results of point source detection and spectra of the bright X-ray sources. In Sec. 4 we present our analysis for the detection of diffuse X-ray emission. Section 5 discusses the point sources tentatively identified as members of NGC 55, followed by a discussion of the detection of weak diffuse X-ray emission and its comparison with observations at other wavelengths. In an appendix we provide brief information about all the point sources and possible optical counterparts.

2. THE DATA

The *ROSAT* Position-Sensitive Proportional Counter (Pfeffermann *et al.* 1987) imaged NGC 55 for 18.9 ksec in 12 observation intervals spread across 122 ksec (≈ 1.5 days) of real time during 1991 November 22–24 (Table 1). We obtained the data from the HEASARC (observation number wp600107), where it had become public on 1995 June 1. The investigation of long-term trends will not be possible because of the short observational timespan. Figure 1 shows an event image of nearly the entire PSPC field-of-view. The faint white arcs and straight bands are the window support structure of the detector. The straight bands are those window support ribs that are parallel to the direction of the satellite wobble. The radius of the "main ring" of the support structure is $\sim 20'$. NGC 55 lies at the center of the field; its optical and radio emission extends nearly parallel to the telescope wobble. The point-like sources that have been detected (to be described shortly) are identified by number; the

[1]Code 660.2, NASA-Goddard Space Flight Center/Universities Space Research Corporation, Greenbelt, MD 20771.
[2]Current address: Center for Astrophysics, Mail Stop 4, 60 Garden St., Cambridge, MA 02138.
[3]Tata Institute of Fundamental Research, Homi Bhabha Road, Mumbai 400005, India.

 0004-6256/97/113(4)/1296/14/$10.00

TABLE 1. Summary of NGC 55.

Position of NGC 55	
RA (J2000)	00:15:08.5
Dec (J2000)	−39:13:13.3
Galactic Column: 1.55×10^{20} cm^{-2}	
Adopted distance: 1.6 Mpc	
ROSAT observation:	
Sequence	WP600107
Exposure	18.9 ksec
Observation Date	1991 Nov 22–24

crowded center region is expanded in Fig. 2 (see below).

The energy spectrum was divided into the seven bands as defined by Snowden *et al.* (1994) where energy bands 1–7 are given by channels 11–19, 20–41, 42–51, 52–69, 70–90, 91–131, and 132–201, respectively. Following Snowden *et al.* (1994), we ignore band 3 (near the carbon edge) because it has a mixed response of the 1/4 and 3/4 keV bands. Very little information is lost by ignoring this band because of its very low count-rate. Table 2 lists the raw and net (after screening) counts across the entire NGC 55 observation. Images were produced by adding bands 1+2, bands 4+5, and bands 6+7 to produce 0.25, 0.75, and 1.5 keV images, respectively. The reader is referred to Fig. 2 in Snowden *et al.* (1995) for energy response curves for the bands chosen here. A fourth image was created by summing the entire energy range. Source detection was then applied to these three images. After the screening, a total of 17.66 ksec remained.

3. ANALYSIS AND RESULTS

3.1 Point Source Detection

Point-like sources were detected using two methods: a sliding box routine in which the background is defined locally and a maximum likelihood algorithm (available in the PROS analysis package). The two approaches were used to provide confidence in the final list of detected sources. The PROS detection algorithm operates on the original event list. We filtered the event list to provide the same three energy bands as were generated by the background modeling code as described above. The sliding box routine was used on the output of the Snowden algorithm (Snowden *et al.* 1994) for handling the X-ray background. The largest differences in the lists of detected sources occurred in the outer regions of the detector. Consequently, no sources beyond a radius of ~50′ from the optical axis nor weaker than a threshold of 5σ are considered.

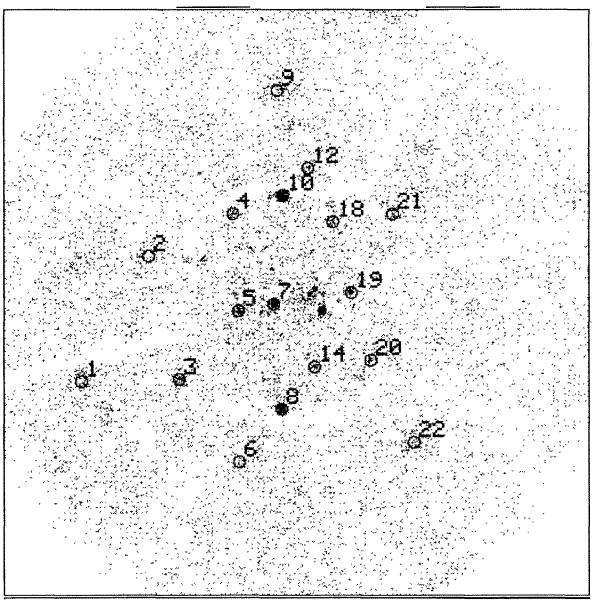

FIG. 1. Event image of the NGC 55 pointing covering the energy range of 0.2–2.4 keV. North is up and east is to the left. The white arcs (north, south) and bands (east, west) are the window support structure for the PSPC. The diameter of the white arcs is ~40′ which establishes the scale of the image. The sources are numbered as in Table 3. The crowded center region is expanded in Fig. 2.

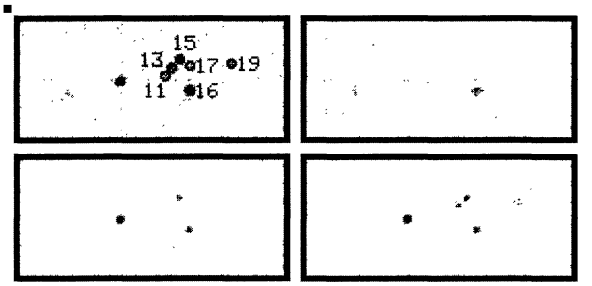

FIG. 2. Image of the immediate region around NGC 55; the galaxy is oriented essentially parallel to the long axis of the image. These images have been cleaned of contaminating background and particle events. The images are (upper left) summed image for the full band from 0.2–2.4 keV; (upper right) the 0.25 keV band; (lower left) the 0.75 keV band; and (lower right) the 1.5 keV band. The small black square represents the north-east corner. The images are 32′ by 16′ in size.

3.2 The Sources, en masse

The source detection algorithms gave the following results. Twenty-five sources were detected in the 0.25 keV band of which three sources were deemed spurious because they lay too near the edge of the detector or under one of the window support ribs. Twenty sources were detected in the 0.75 keV band and 24 sources were detected in the hard band where, again, two sources were deemed spurious because they lay too close to the detector edge. Most of these sources fall well beyond the "boundary" of NGC 55, but we have chosen to number them uniquely and to use those numbers throughout this paper. Our final list contains 22 sources. Eight of these sources viz., source numbers 5, 7, 11, 13, 15,

TABLE 2. Counts in each band.

Band	Approx. Energy Range (keV)[a]	Total Counts[b]	Modeled Background Counts	Net Counts[c]
1	0.11–0.28	39508	6306.9	33201.1
2	0.14–0.28	55499	5964.3	49534.7
4	0.44–1.01	8008	988.1	7019.9
5	0.56–1.21	9117	2172.6	6944.4
6	0.73–1.56	10452	2275.1	8176.9
7	1.05–2.04	6210	2864.8	3345.2

[a]Band definitions from Snowden *et al.* (1994).
[b]Total counts from all sources, including particle background and solar scattered X-rays.
[c]Counts after screening using *S*. Snowden's particle background and scattered X-ray modeling code (Snowden 1995).

TABLE 3. Point sources in NGC 55.

No.	J2000 RA[a]	J2000 Dec[a]	Offaxis Angle (′)	Soft Counts	Hard Counts	HR[b]	Flux[c]	In NGC 55?[d]
1	00 18 24.4	−39 26 24	40	78 ± 27	107 ± 20	0.16 ± 0.19	9	U
2	00 17 22.4	−39 04 46	26	<20	65 ± 15	>0.53	5	B?
3	00 16 55.4	−39 26 45	24	78 ± 22	98 ± 16	0.12 ± 0.16	9	U
4	00 16 06.6	−38 57 39	19	<21	40 ± 15	>0.31	4	B?
5	00 16 01.5	−39 14 41	10	200 ± 21	21 ± 11	−0.80 ± 0.09	31	M?
6	00 15 42.2	−39 40 04	28	<26	47 ± 17	>0.29	4	B?
7	00 15 29.2	−39 13 25	4	57 ± 17	3331 ± 59	0.96 ± 0.01	750	M?
8	00 15 23.3	−39 31 50	14	145 ± 24	276 ± 21	0.31 ± 0.08	45	F?
9	00 15 22.5	−38 35 49	38	165 ± 28	84 ± 17	−0.32 ± 0.12	12	F?
10	00 15 22.2	−38 54 35	19	282 ± 27	183 ± 19	−0.21 ± 0.06	27	F?
11	00 15 01.0	−39 12 53	0	<10	115 ± 13	>0.84	14	M
12	00 14 58.3	−38 49 42	24	40 ± 21	<13	<−0.50	2	F?
13	00 14 57.2	−39 11 48	0	<9	223 ± 17	>0.93	56	M
14	00 14 52.2	−39 24 21	12	87 ± 18	45 ± 12	−0.35 ± 0.15	6	B?
15	00 14 52.1	−39 10 52	0	<10	445 ± 23	0.95	27	M
16	00 14 46.1	−39 14 38	5	388 ± 25	582 ± 27	0.22 ± 0.03	69	F
17	00 14 45.2	−39 11 32	0	<10	76 ± 11	>0.76	9	M?
18	00 14 37.0	−38 59 11	15	<21	54 ± 15	>0.44	5	B?
19	00 14 20.1	−39 11 18	10	<20	140 ± 18	>0.75	17	M
20	00 14 08.2	−39 23 49	17	40 ± 21	72 ± 15	0.35 ± 0.26	7	U
21	00 13 41.4	−38 57 38	23	23 ± 26	66 ± 18	0.54 ± 0.47	6	U
22	00 13 24.1	−39 37 33	32	101 ± 28	96 ± 19	−0.04 ± 0.16	11	F?

[a]Source positions will be poor if the source lies near one of the structural supports of the PSPC, or if the source lies at a large off-axis angle. Source positions that may be affected by the structural supports are sources 1, 3, 4, 8, 10, 12, 20, and 21; source positions that may be affected by the large off-axis angle are sources 1, 9, and 22.

[b]HR, the hardness ratio, is defined as (H−S) / (H+S).

[c]Approximate flux, in units of 10^{-14} ergs s^{-1} cm^{-2}, based on spectral fitting or two input models. For the bright sources, the flux from the best-fit spectrum (Table 4) is listed. For the fainter sources, two input models have been adopted. The first model, applied to all Members (certain or not) of NGC 55, is a thermal bremsstrahlung with kT = 1 keV and $N_H = 5\times10^{20}$ cm^{-2}. The model norm is adjusted to match the count rate and the flux is computed in the 0.2–2.4 keV band after setting N_H = 0.0. The second model, applied all remaining sources, is a thermal bremsstrahlung with kT = 1 keV and $N_H = 1.55\times10^{20}$ cm^{-2}. The model norm is adjusted to match the count rate and the flux is computed in the 0.2–2.4 keV band after setting N_H = 0.0. Note that the adopted values for the column may under- or over-estimate the true column to the source.

[d]F = Foreground object, M = Member of NGC 55, U = Unknown, B = Background object. None of the identifications are certain, however, a question mark indicates additional uncertainty in the assignment of location.

16, 17, and 19 are positionally coincident with NGC 55. The remaining 14 sources are either foreground or background objects. Based on the log N–log S relation of Hasinger *et al.* (1991), we expect between 10 and 20 extragalactic sources to lie in the NGC 55 field.

Many of the sources are too weak for detailed analyses such as spectral fitting or timing studies. To estimate the shape of the spectrum, we define a hardness ratio such that $HR=(H-S)/(H+S)$, where H represents the sum of the counts in the 0.75 and 1.5 keV bands and S represents the counts in the 0.25 keV band. Table 3 lists the positions of the detected sources in *de*creasing RA order, the counts in the soft and hard bands, and the hardness ratio. Table 3 also lists the flux in the 0.2–2.4 keV energy band. For the bright sources, the flux has been calculated from the fitted spectrum after setting the column density to zero. For the weak sources we have calculated the flux assuming one of two models. Both models adopt a 1 keV thermal bremsstrahlung for the continuum. The models differ in the value of the adopted N_H, with values of 10^{20-21} cm^{-2} for those sources deemed to be members of NGC 55 and a value of 1.55×10^{20} cm^{-2} (Stark *et al.* 1992) for those sources deemed to be unassociated with NGC 55. We have created this division so we can generate reasonable fluxes for the NGC 55 sources. The definition of the phrase "unassociated with NGC 55" is strictly based on the angular separation from NGC 55 for the weak sources. All sources outside of 5′ from the central plane of NGC 55 are deemed to be foreground or background objects.

Figure 2 shows excised portions of the background-corrected (Snowden 1995; Snowden *et al.* 1994) PSPC data in the region around NGC 55. The gray-scale image has been scaled to emphasize the point sources. The panel in the upper left shows the 0.2–2.4 keV band with the sources identified by number; the other panels are the 0.25 keV band (upper right), the 0.75 keV (lower left), and the 1.5 keV band (lower right). Source 5 is clearly visible only in the 0.25 keV band while source 19 is just barely visible in the 0.75 keV band but clearly visible in the 1.5 keV band. From this image, we can see the range of spectral hardness exhibited by several sources.

3.3 X-ray Spectra of the Bright Sources

Eight sources were deemed sufficiently bright (>200 counts) to merit spectral fitting (described in the next sec-

TABLE 4. Spectral fit parameters.

No.	Model	χ^2	ν	N_H (10^{20} cm^{-2})	kT or Γ	F_X[a] (ergs s^{-1} cm^{-2})
5	Blackbody	11.5	12	$6.5^{+30}_{-3.0}$	$0.023^{+0.03}_{-0.023}$	3.1(−13)
	Power law	11.7	12	$3.05^{+\infty}_{-1.0}$	$4.56^{+\infty}_{-0.3}$	...
	Bremsstrahlung	11.6	12	$2.29^{+4.0}_{-1.0}$	<0.30	...
7	Blackbody	20.8	23	$8.7^{+4.0}_{-2.5}$	$0.29^{+0.02}_{-0.02}$	...
	Power law	15.8	23	$30.1^{+0.8}_{-0.4}$	$2.92^{+0.50}_{-0.30}$	...
	Bremsstrahlung	16.1	23	$20.8^{+5.0}_{-4.5}$	$0.98^{-0.4}_{-0.2}$	7.5(−12)
8	Blackbody	15.9	23	<8	$0.19^{+0.04}_{-0.03}$	...
	Power law	16.8	23	$4.7^{+2.0}_{-2.0}$	$2.68^{-0.7}_{-0.7}$	...
	Bremsstrahlung	16.0	23	$3.0^{+1.4}_{-1.2}$	$0.68^{+0.75}_{-0.24}$	4.5(−13)
9	Blackbody	9.5	11	<1	$0.15^{+0.03}_{-0.02}$	...
	Power law	9.5	11	$2.16^{+0.05}_{-0.04}$	$2.59^{+1.84}_{-1.84}$	...
	Bremsstrahlung	9.6	11	$1.04^{+0.03}_{-0.02}$	<2.3	2.7(−13)
10	Blackbody	33.3	23	$6.58^{+0.08}_{-0.07}$	$0.025^{+0.018}_{-0.018}$	...
	Power law	17.5	23	$1.90^{+1.6}_{-1.0}$	$2.69^{+1.0}_{-0.6}$	...
	Bremsstrahlung	19.4	23	$1.25^{+0.75}_{-1.22}$	$0.48^{+0.65}_{-0.14}$	2.7(−13)
13	Blackbody	8.6	11	$6.3^{+2.0}_{-2.0}$	$0.49^{+0.34}_{-0.34}$	...
	Power law	9.7	11	<40	$1.39^{+1.23}_{-1.23}$	...
	Bremsstrahlung	8.0	11	37^{+30}_{-17}	$1.13^{+\infty}_{-0.42}$	5.6(−13)
15	Blackbody	11.7	11	<1	<4.2	...
	Power law	9.1	11	<44	$2.14^{+1.38}_{-1.38}$	...
	Bremsstrahlung	10.8	11	$21.4^{+17.5}_{-17.5}$	$1.20^{+1.28}_{-1.28}$	2.7(−13)
16	Blackbody	13.0	23	<0.002	$0.198^{+0.1}_{-0.1}$	...
	Power law	15.8	23	$3.0^{+1.0}_{-0.7}$	$2.30^{+0.27}_{-0.25}$	...
	Bremsstrahlung	11.8	23	$1.9^{+0.6}_{-0.5}$	$0.92^{+0.2}_{-0.5}$	6.9(−13)
Diffuse	Bremsstrahlung	35.8	60	$0.026^{+0.010}_{-0.004}$	$1.0^{+0.6}_{-0.1}$	9.9(−13)

[a]The flux is calculated in the 0.2–2.4 keV band after setting N_H to zero.

tion). The counts for each of these sources were extracted to create binned spectra. The number of bins ranged from 11 for sources with fewer than 400 counts to 25 for the brightest source. Each spectral bin contained at least 15 counts. Vignetting corrections were included in the spectral fitting process. Three continuum models were fit to each spectrum: blackbody, thermal bremsstrahlung, and power law. In general, there were insufficient counts to warrant additional spectral components. The calculated fluxes are insensitive to the specific, fitted spectrum because the signal-to-noise ratio is low. For convenience, we adopt the thermal bremsstrahlung model as the best-fitting model unless we state otherwise. For the spectral fits, we used version 9 of "xspec." Table 4 lists the spectral parameters of the fits for each source. We examined the optical image of NGC 55 (not shown, but obtained from the Skyview facility at the HEASARC[4] and we make brief comments about possible optical counterparts. We now turn to a brief description of the bright sources.

Source 5 has the softest spectrum and is the ultra-soft X-ray source identified in the catalog of soft sources by Singh *et al.* (1995). The blackbody model provided the best fit to the data with a $kT \sim 23$ eV. There is no evidence for a hard component in the spectrum. Figure 3 shows the fitted blackbody spectrum and the parameter contours. The X-ray position lies just north of the plane of NGC 55; the stellar density is still high at this location, hindering the identification of a counterpart.

Source 7 differs from the other sources for which spectra can be extracted. The fitted spectrum shows evidence for a high column density, regardless of the adopted model, with N_H approximately an order of magnitude higher than for any other source ($\sim 2\times10^{21}$ cm^{-2}). The fitted bremsstrahlung temperature is approximately 0.8 keV. If we adopt a power law model, the fit describes the data as well as the bremsstrahlung model and yields a photon index of ~2.5–3.5. If the continuum is modelled with a blackbody, the temperature is ~0.28 keV and is relatively tightly constrained. Figure 4 shows the spectrum and the parameter contours. Source 7 lies just north of the plane of NGC 55, so the identification of the optical counterpart will be difficult.

Source 8 was equally well-fit by any one of the three continuum models. The column density is low, $\sim 3\times10^{20}$ cm^{-2} but is consistent with the Galactic column regardless of the adopted model. The bremsstrahlung temperature is approximately 0.7 keV, while the blackbody temperature is ~0.2 keV. The power law photon index is ~2–3.5. Figure 5 shows the spectrum and the parameter contours. A star-like object lies at the X-ray position but it is unclear from the optical image whether the potential counterpart is a foreground star.

Source 9 has too few counts for a tightly-constrained fit. A blackbody model yielded the tightest constraints on the model spectrum. The column density is essentially unconstrained, but the temperature is <1 keV. Figure 6 shows the spectrum and the parameter contours. The optical image reveals no counterparts near the X-ray position.

Source 10 is a moderately soft source (hardness ratio

[4]Skyview: http://skyview.gsfc.nasa.gov/

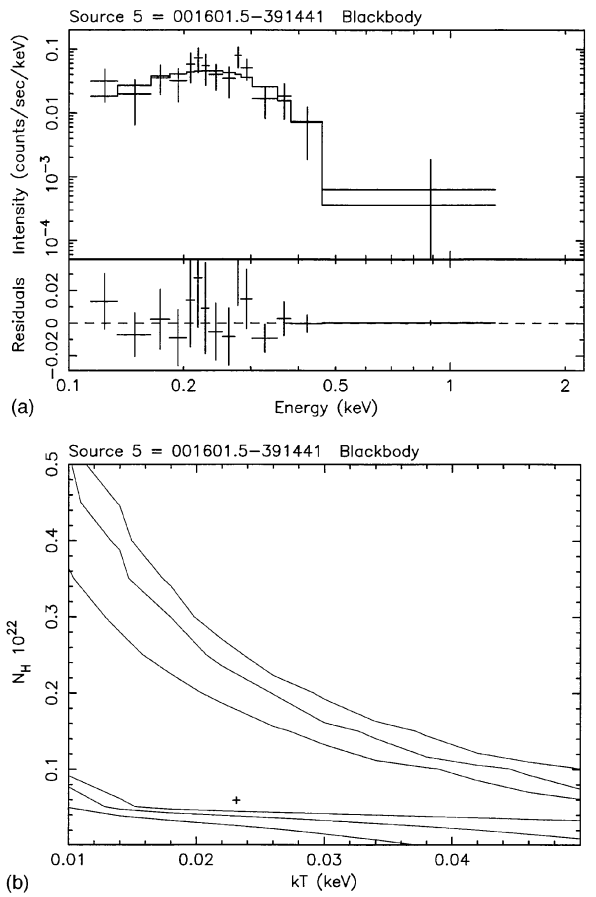

FIG. 3. Fitted spectrum (a) and contours (b) for source 5. The contours, used for all spectral fitting, are the $\Delta\chi^2$ increments of 2.3, 4.71, and 9.21 which represent the 68%, 90%, and 99% confidence levels for 2 parameters of interest.

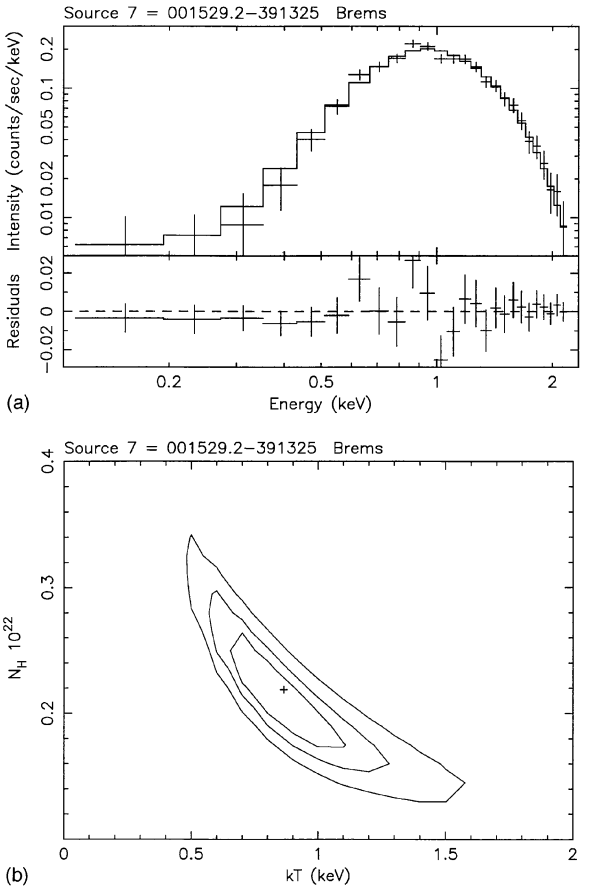

FIG. 4. Fitted spectrum (a) and contours (b) for source 7.

$\sim -0.21 \pm 0.06$). If a thermal bremsstrahlung model is used to fit the data, the fitted column density is $\sim 10^{20}$ cm^{-2} while the fitted temperature is ~0.5–1 keV. A power law model provides an equally good fit with a similar column density and a photon index of ~2–3.5. Figure 7 shows the spectrum and the parameter contours. One or two likely optical counterparts exist.

The spectrum of Source 13 does not constrain the model parameters. For a bremsstrahlung spectrum, the temperature is >0.5 keV; the column density is greater than the Galactic column density by a factor of at least an order of magnitude implying a location in the plane of NGC 55. Figure 8 shows the spectrum and the fitted contours. The hardness of the spectrum and the association with NGC 55 suggest that the source is an X-ray binary. The optical field is very crowded, so the identification of the counterpart will be difficult.

The spectrum of source 15 is very similar to that of source 13, except that the fitted temperature is tightly constrained to be >0.6 keV. The column density is also an order of magnitude higher than the Galactic column density. The comments made above for source 13 apply equally well here. Figure 9 shows the spectrum and the fitted contours.

Source 16 appears to be identical to source 8 based on the fitted spectrum. The column density is low, $\sim 2\times 10^{20}$ cm^{-2} while the bremsstrahlung temperature is approximately 1 keV. The blackbody and power law models provide visibly poorer fits, even though χ^2/ν is approximately the same, because a clear residual pattern exists. For the power law fit, for example, residuals are present near 1 keV. Figure 10 shows the spectrum and the fitted contours. An apparent foreground star lies at the X-ray position.

The bright sources were all examined for variability on times of less than a day using a two-sided Kolmogorov-Smirnov (K-S) test. Sources 5, 10, and 15 did not show any evidence for variability at the 99% confidence level. Variability was detected in sources 8 and 16 at the 95% level but not at the 99% level. Only source 7 showed evidence for variability at the 99% confidence level. We then looked for power at a particular frequency, but aside from the power introduced by the satellite wobble (400 sec and its aliases) and the satellite sampling frequency (~95 min), no power at any frequency from 1 to 20 μHz was convincingly detected. We conclude that none of the bright sources showed evidence for variability during the PSPC observation.

4. DIFFUSE X-RAY EMISSION

The galaxy is physically large on the sky (~20′), so the contributions of the particle background, solar-scattered

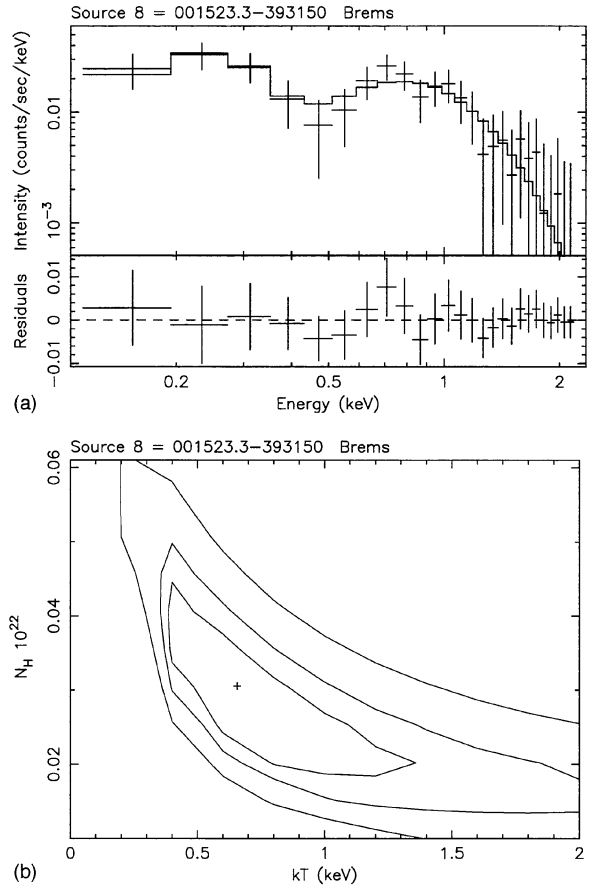

FIG. 5. Fitted spectrum (a) and contours (b) for source 8.

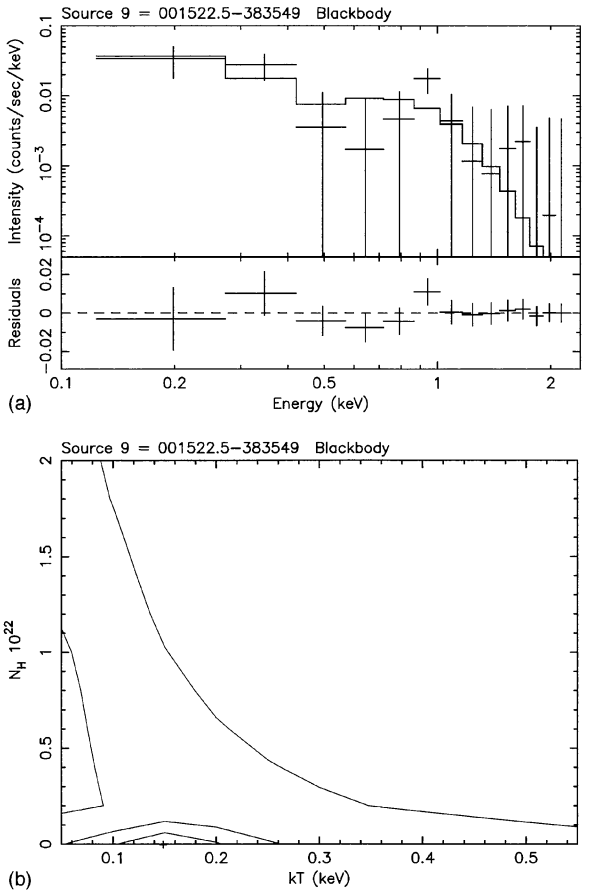

FIG. 6. Fitted spectrum (a) and contours (b) for source 9.

X-rays, the instrumental vignetting, and short- and long-term enhancements must be properly removed from the data before analysis. An easy approach to meet this requirement is the use of S. Snowden's software[5] that was developed to analyze extended objects or large regions of diffuse emission (Snowden 1995). It screens out the contributions from each of the above-listed contaminants leaving net counts properly corrected for vignetting. Applications of the software have been described in Snowden & Pietsch (1995), for M101, and Snowden *et al.* (1995) for the diffuse galactic emission.

The reader can see from Figs. 1 or 2 that any diffuse emission is weak or non-existent. Diffuse emission is expected to arise from the integrated emission along the line of sight. For an edge-on galaxy, this emission will lie above and below the plane of the galaxy as a hot halo, or lie in the plane of the galaxy as a narrow band of emission, similar to the diffuse X-ray emission detected in the edge-on galaxies NGC 891 (Bregman & Pildis 1994) or NGC 4631 (Wang *et al.* 1995). For a hot halo, the softer energies are most likely to show evidence for diffuse emission for two reasons. First, the Galactic column density in the direction of NGC 55 is very low (near the South Galactic Pole) so relatively few of the soft photons will be absorbed before reaching the detector. Second, the hot diffuse emission is expected to have a peak either in the soft X-ray band or a tail extending into the soft X-ray band from the EUV. The gas is believed to have a temperature of $\sim 10^{6-7}$ K. It is possible that a distribution of temperatures is present but there is, as yet, no evidence for such a distribution.

Figure 11 shows the X-ray "diffuse" emission of NGC 55 in the 0.25, 0.75, and 1.5 images as well as the summation of these images. The images have all been generated using the Snowden code, as was done in Fig. 2, with the additional operations of cutting out the emission from the detected point sources (the white squares) and adaptively smoothing the remainder. For all of the images, the number of counts in the smoothing kernel was set at 100. The reader should interpret this image with caution because the quality of the background subtraction will clearly affect the conclusions that may be drawn. We believe the background has been correctly subtracted; a slight change, however, in the subtraction would affect the lowest gray levels (Fig. 11) or contours (Figs. 13 and 14).

The 0.25 keV image (Fig. 11, upper right) may be consistent with random fluctuations of the diffuse Galactic emission because no emission appears strongly and preferentially distributed around NGC 55. The average value of the 0.25 keV soft X-ray emission (Snowden *et al.* 1996, 1995) in the direction of NGC 55, as extracted in a 10° region surrounding the PSPC field but excluding NGC 55, is $\sim 8.9 \times 10^{-4}$

[5]Standalone Fortran code, available via FTP from NASA-GSFC.

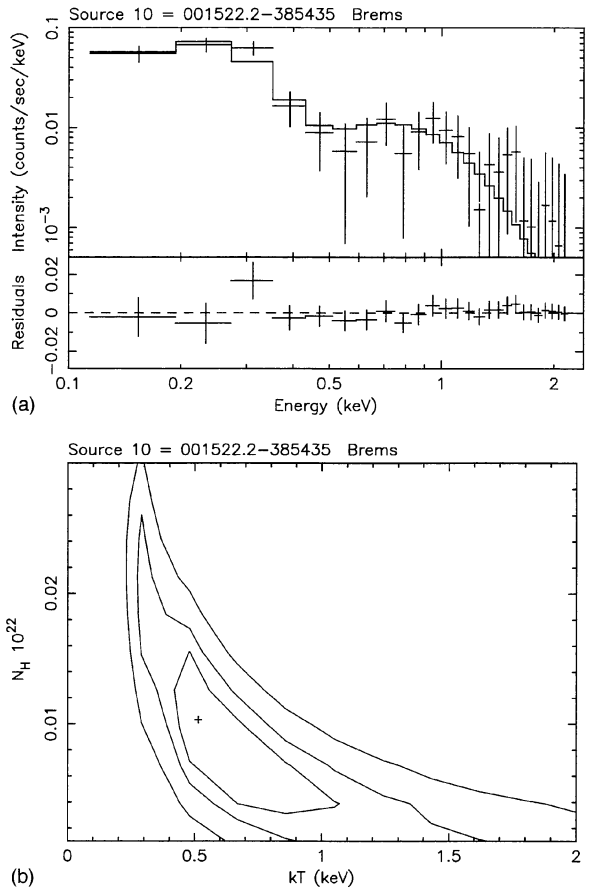

FIG. 7. Fitted spectrum (a) and contours (b) for source 10.

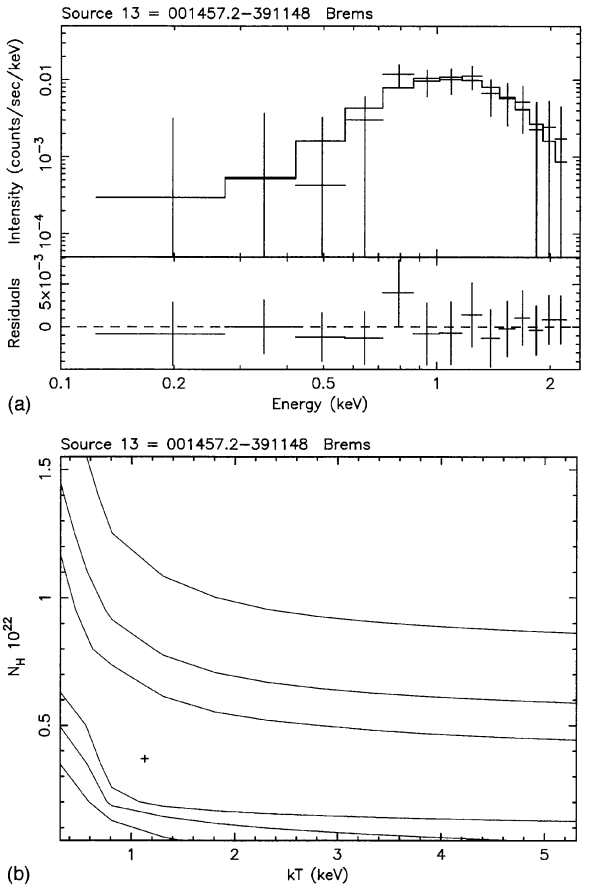

FIG. 8. Fitted spectrum (a) and contours (b) for source 13.

counts s^{-1} $arcmin^{-2}$. Emission at this level easily overwhelms diffuse emission of NGC 55 itself in the 0.25 keV band. Evidence that NGC 55 casts a shadow from the extragalactic 0.25 keV emission is presented in Barber *et al.* (1996) using the *ROSAT* PSPC observation of NGC 55. We refer the reader to that paper for an excellent and detailed analysis.

For the 0.75 and 1.5 keV images, however, emission in the plane of the galaxy is visibly present. Our immediate goal is the overlay of contours of X-ray emission onto optical, radio, and other images of NGC 55. We set the X-ray contour levels by extracting the counts in each energy band in a cut perpendicular to the plane of the galaxy and centered just east of the optical center. This position avoided all of the detected X-ray sources. We used rectangular apertures of size 0.5 by 2.5 and extending 7′ outward from the plane. The counts in each aperture were summed and the results are plotted in Fig. 12. The mean level and its standard deviation were calculated by averaging the counts in the outer apertures. The apertures were chosen from an examination of the 0.75 keV profile, which is a most cleanly defined profile, after ignoring any weak point sources. Identical apertures were used for all three bands. Contour levels for the X-ray overlays were then chosen based upon this mean level. The emission in the 0.25 keV band is consistent with the Galactic 0.25 keV emission and the extragalactic 0.25 keV background.

Figure 13 shows an overlay of the contours of the 0.75 keV data on an optical image of NGC 55. The lowest contour shown marks the level of ~1.3 times the mean background level. The average value of the 0.75 keV flux from the cosmic X-ray background in this direction is $1.1 \pm 0.1 \times 10^{-4}$ counts s^{-1} $arcmin^{-2}$. (Snowden *et al.* 1996, 1995). The 0.75 keV emission is largely confined near the plane of NGC 55, perhaps extending slightly above and below the plane as defined by the optical image. Note that at least one of the excluded regions surrounds an apparent foreground star (just west of 0:15, -39:15).

The *IRAS* 60 μm and 100 μm images of NGC 55 (not shown) essentially match the inner contours of the 1.5 keV image in morphology. The emission is confined to the disk plane and is devoid of any plumes or other structure. The 12 and 25 μm emission (not shown) are essentially confined to the region surrounding sources 11, 13, 15, and 17. No emission is apparent in the region surrounding source 7 that lies to the east (Rice 1993). We also do not present overlays of the X-ray contours onto the [S II] or Hα images from Hoopes *et al.* (1996). In their paper, they show that the [S II] diffuse emission is present near regions of star formation. For NGC 55, the [S II] and Hα emission clusters near source 7 and near sources 11, 13, 15, and 17, so it is very similar in ap-

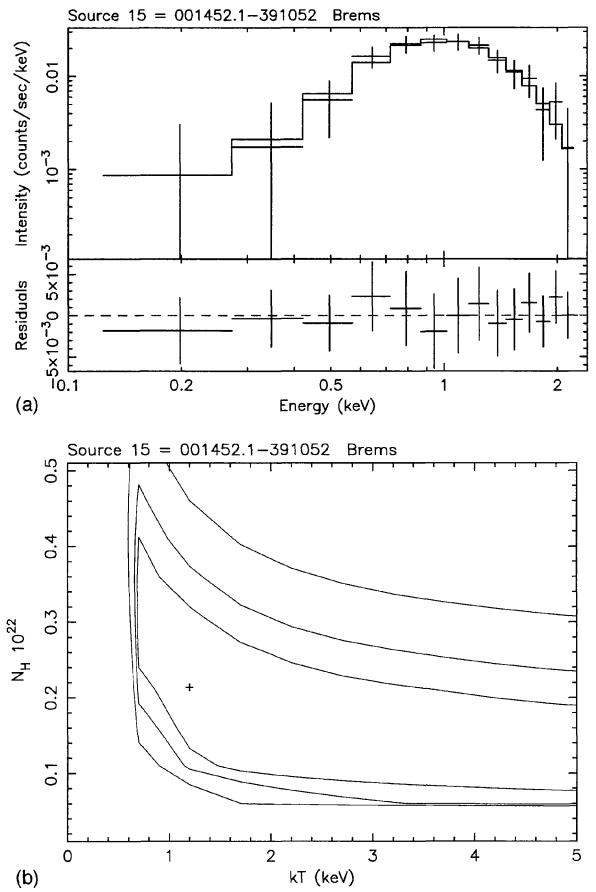

FIG. 9. Fitted spectrum (a) and contours (b) for source 15.

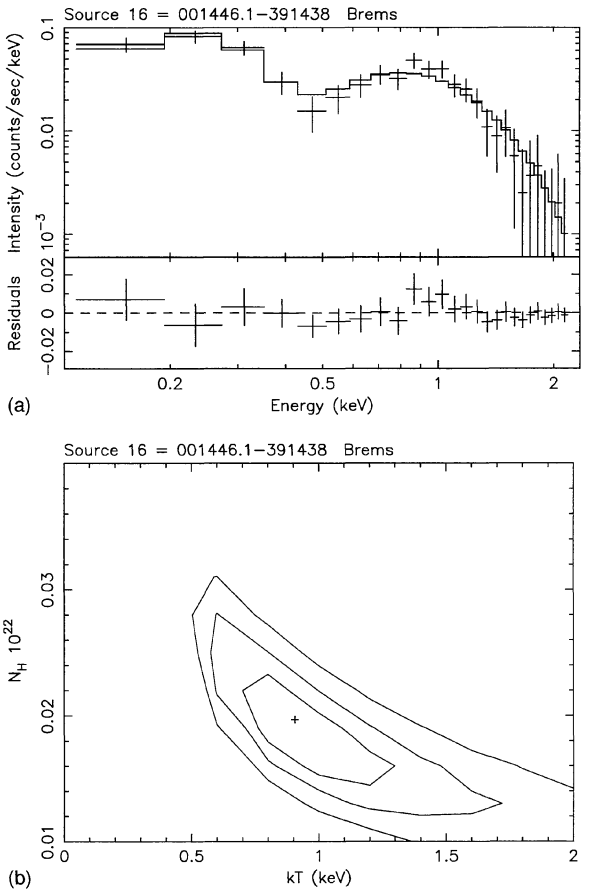

FIG. 10. Fitted spectrum (a) and contours (b) for source 16.

pearance to the innermost X-ray contours of Fig. 13.

Figure 14 shows an overlay of the contours of the X-ray data (1.5 and 0.75 keV) onto the H I map obtained from Very Large Array H I measurements (Puche *et al.* 1991, hereafter PCW91). The most striking structure is the south-pointing plume (RA 0:15:39, Dec −39:20) in the 0.75 keV band, but which is not visible in the 1.5 keV band. The X-ray plume shares the same direction and morphology as the radio plume, but appears to lie inside of the radio plume. The H I plume has a surface density of $\sim 5\times 10^{19}$ cm^{-2} as measured from the VLA image. At the adopted distance to NGC 55, the X-ray plume has a length of $\sim 3'$ which corresponds to ~ 1.4 kpc. If we assume that the plume has a circular cross-section, the radius is $\sim 30''$ or ~ 0.25 kpc.

Figure 15 shows the spectrum and the parameter contours for the diffuse emission. The spectrum was extracted by placing a box around the entire galaxy, oriented as the galaxy is on the sky, and removing from the boxed emission the emission from each of the point sources. The reader should note that the point sources were constrained to be detected at better than the 5σ level so, undoubtedly, some of the "diffuse" emission represents the emission of sources weaker than that detection level, particularly near sources 11 and 13. The fitted spectrum, corrected for vignetting, can be described as a moderately absorbed continuum with a bremsstrahlung temperature of ~ 1 keV. The resulting X-ray unabsorbed flux in the 0.2–2.4 keV band is 9.8×10^{-13} ergs s^{-1} cm^{-2}. For the adopted distance, this flux corresponds to a luminosity of $\sim 3\times 10^{38}$ ergs s^{-1}.

5. DISCUSSION

In this section, we discuss, first, the point sources, and second, the diffuse emission.

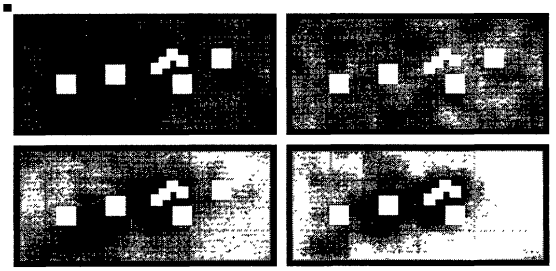

FIG. 11. Image of the immediate region around NGC 55. This figure is similar to Fig. 2 except that the point sources have been cut out and the remainder has been adaptively smoothed (see Sec. 4). Size and arrangement are as in Fig. 2.

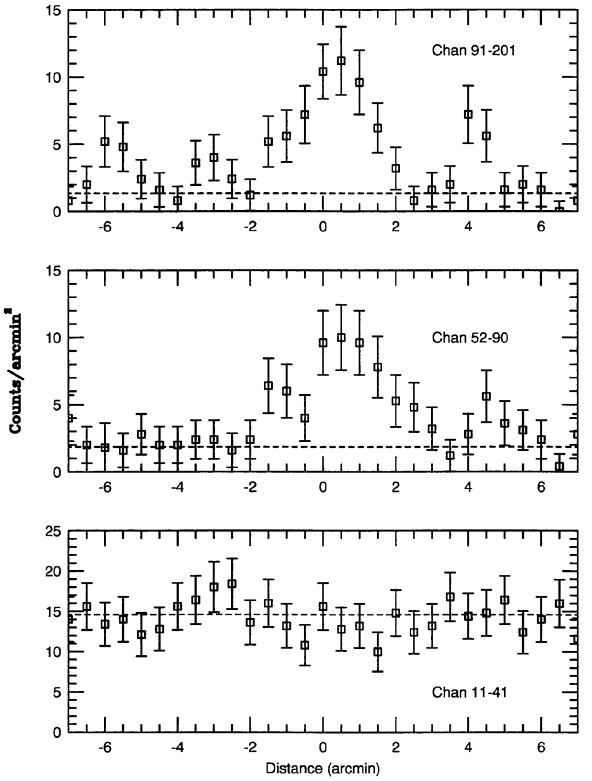

FIG. 12. Plot of the rectangular cut made perpendicular to the plane of the galaxy (described in Sec. 4). The mean level in each band is indicated by the dashed line.

5.1 Point-like X-ray Sources in NGC 55

The column density of H I gas in our galaxy towards the direction of NGC 55 is known to be $\sim 1.55\times10^{20}$ cm^{-2} (Stark *et al.* 1992), so values of the fitted column density of point sources significantly different from that value must be reflected in our interpretation of the data. The detected point sources can be divided into three groups: (i) those not associated with NGC 55, (ii) those apparently associated with NGC 55 but possessing a low value for the fitted column density, and (iii) those apparently associated with NGC 55 but possessing a high value for the fitted column density. We defer any discussion of the unassociated sources to the appendix. The sorting is done on the basis of the angular separation from the disk plane, the value of the fitted column (if available), the appearance of the optical finding chart, and the value of the hardness ratio. The angular separation carries the most weight. We stress that our segregation of the sources is a proposed separation; optical spectroscopic observations are necessary to confirm our division of the detected sources. For those sources with a high value for the column density, we can compare the fitted values with surface density maps of the H I gas in NGC 55 using the data of PCW91.[6] The highest value in the map is 8.7×10^{21} cm^{-2} which is located about 1′ SE from the optical maximum.

Source 5 lies on the edge of the contour at 1×10^{21} cm^{-2} in PCW91, consistent within the errors with the fitted column density from the X-ray spectrum. The consistency of the columns from the X-ray and the radio suggests that source 5 must be associated with NGC 55 or be positioned beyond it. The unabsorbed 0.2–2.4 keV luminosity, assuming the source is associated with NGC 55, is $\sim9\times10^{37}$ ergs s^{-1}. Note, however, that source 5 is very soft, so the luminosity is a very sensitive function of the column density. The association of source 5 with NGC 55 is the most straight-forward interpretation of the data.

The recent release of the *ROSAT* All-Sky Survey Bright Source Catalog (Voges *et al.* 1996) and the public availability of the *HRI* observation of NGC 55 provide us with the opportunity to look at the long-term variability of these sources. The one surprise in the *HRI* image is the absence of source 5. Although the *HRI* has a higher internal background

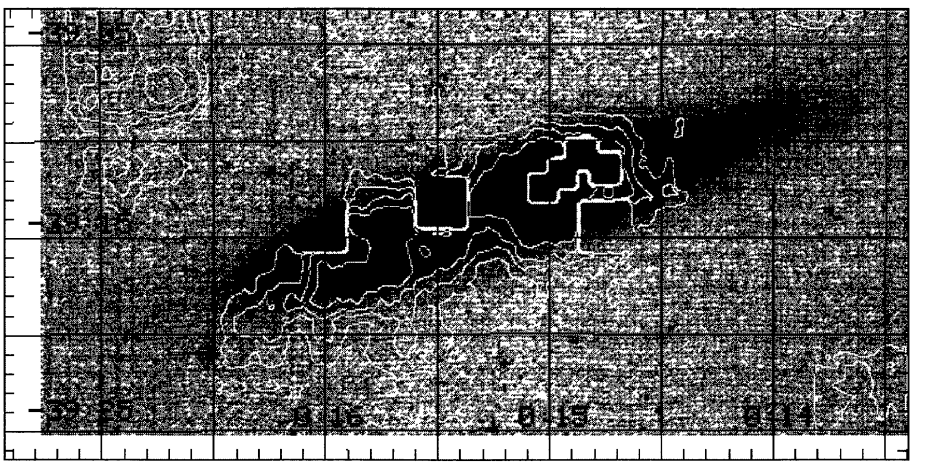

FIG. 13. Overlay of the PSPC 0.75 keV data (contours) from Fig. 11 on an optical image of NGC 55 (optical image from digitized Palomar Sky Survey, obtained from the Skyview tool at the HEASARC). The contours mark the levels of 1.3, 1.5, 1.7, and 2.0 times the mean background level of 1.05×10^{-4} counts s^{-1} arcmin^{-2}. These contours correspond approximately to the 1.3σ, 2σ, 3σ, and 4.5σ. The coordinates are J2000.

[6]Their Fig. 4, available on the NRAO CD-ROM "Images from the Radio Universe."

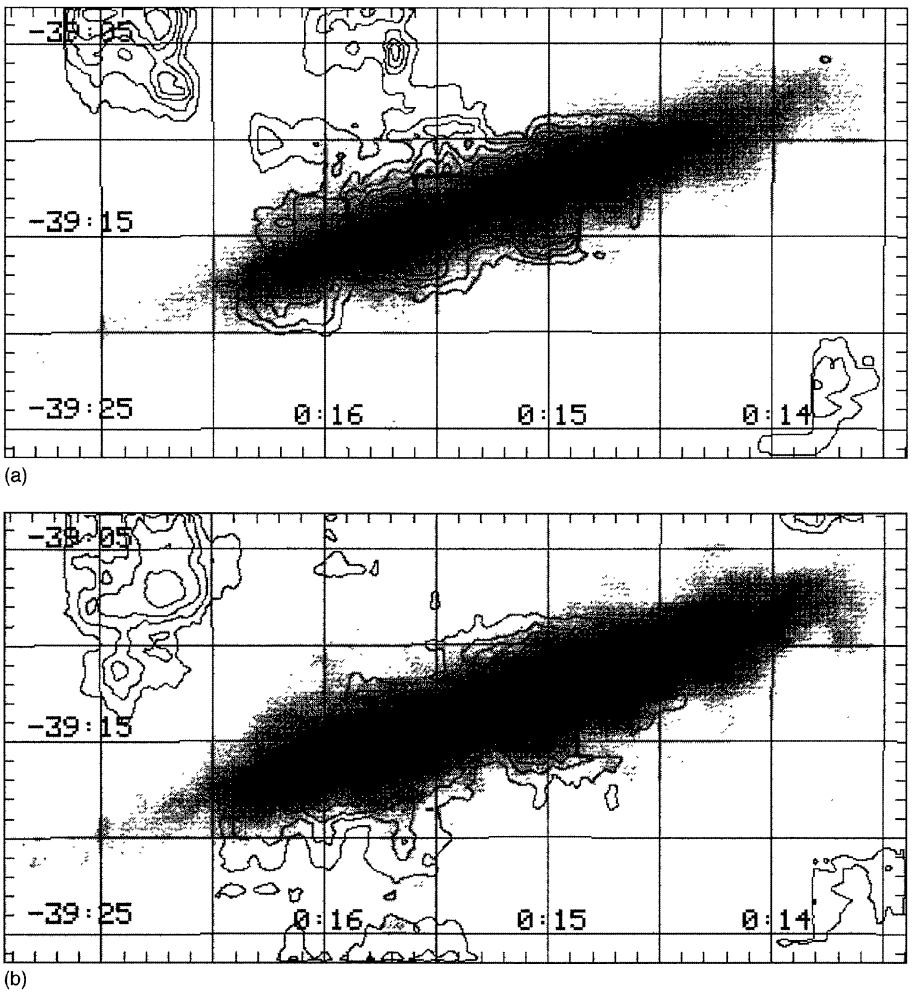

FIG. 14. Overlay of the PSPC data (contours) on a VLA total H I map of NGC 55. (a) 1.5 keV (contour levels at 1.1, 1.3, 1.5, 1.7, and 2.0 times the mean background level of 7.61×10^{-5} counts s^{-1} $arcmin^{-2}$; (b) 0.75 keV (contour levels as in Fig. 13).

than the PSPC, the PSPC count rate of $\sim4.5\times10^{-3}$ counts s^{-1} implies an *HRI* count rate of 1.1×10^{-3} counts s^{-1}, or ~30 counts during the 27.5 ks exposure. Given the *HRI* non-detection, we can estimate an upper limit of $\sim5\times10^{-4}$ counts s^{-1}, implying that source 5 is variable. Possible ultra-soft sources with long-term variability include supernovae, X-ray novae, and super-soft sources. There have been no observed supernovae in NGC 55. Unfortunately, the PSPC spectra can not distinguish between the remaining possibilities. If source 5 is confirmed to be a super-soft source, then it is among the most distant supersoft sources known.

Source 7 also lies on the 1×10^{21} cm^{-2} contour of H I gas. The fitted column density is barely consistent with that value, being about three times larger, and perhaps suggesting that this source lies deep in the plane of NGC 55, lies beyond NGC 55, or is intrinsically absorbed. The spectrum is too soft for an X-ray binary in its normal state. A supersoft state or an X-ray nova-like behavior is not ruled out, however. If we assume the source is an AGN, the fitted value of the power law photon index (2.92 ± 0.40) is slightly high relative to the mean photon index of, for example, BL Lac objects, which have an index of ~2.39 (Sambruna *et al.* 1994). We note, however, that BL Lac objects do not show intrinsic absorption. The index is discrepant with the average index for Seyferts (~1.7) and LINERS (~2.1) (Mushotzky *et al.* 1993), narrow emission line galaxies (~1.45), and broad-line AGNs (~2) (Romero-Colmenero *et al.* 1996), but does lie within the range of narrow-line Seyferts (2.70 ± 0.30; Boller *et al.* 1996). The index is also discrepant with the average photon index of Seyfert 1s (2.26 ± 0.11) and Seyfert 2s (2.45 ± 0.18) from the *ROSAT* all-sky survey data (Rush *et al.* 1996). The luminosity, assuming the source is associated with NGC 55, is $\sim2\times10^{39}$ $D_{1.6}^2$ ergs s^{-1}, where $D_{1.6}$ is the distance in units of 1.6 Mpc. For a distance typical of nearby AGN (e.g., 16 Mpc), the luminosity is $\sim2\times10^{41}$ ergs s^{-1}. This luminosity is $\sim10^{3-5}$ times lower than typical for QSOs, $\sim10^{1-2}$ lower than typical for Seyfert 1s, but is a typical luminosity for LINERs or starburst galaxies (B. Wilkes, private communication). The source could also be a highly luminous supernova remnant such as N103B or N132D in the LMC (Singh *et al.* 1987; Hughes *et al.* 1995)

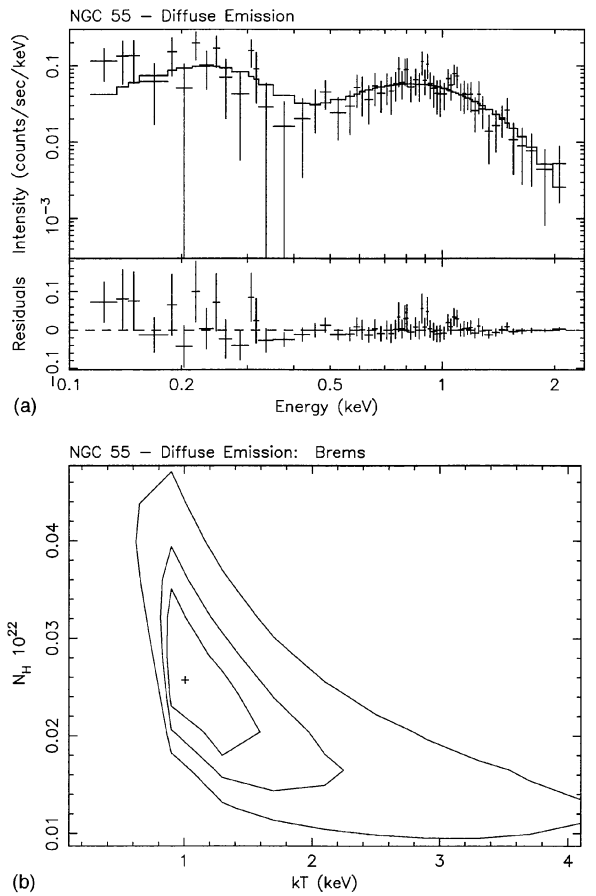

FIG. 15. Fitted spectrum (a) and contours (b) for the emission of the entire galaxy minus the point sources.

based upon the fitted bremsstrahlung temperature and the luminosity.

Sources 13 and 15 are positioned within the 4×10^{21} cm^{-2} contour; the column parameter values derived from fitting the PSPC spectra are consistent with that contour, so both sources are very likely associated with NGC 55. Finally, source 16 lies within the 2×10^{21} cm^{-2} contour. The fitted column density from the X-ray spectrum is about an order of magnitude lower, consistent with the Galactic column density. This result suggests that source 16 is a foreground source. Alternatively, it could be related to NGC 55 but be positioned on the near side of that galaxy. The unabsorbed luminosity, assuming the source is associated with NGC 55, is $\sim2\times10^{38}$ ergs s^{-1}. If we assume the source lies on the edge of our Galaxy and adopt 1 kpc for the distance, the luminosity is $\sim8\times10^{31}$ ergs s^{-1}, consistent with an active star. An examination of the optical image shows that a foreground star lies centered on the X-ray source position. This is most likely the optical counterpart.

Sources 11, 17, and 19 have hardness ratios which are identical to those of sources 7, 13, and 15, possibly indicating common spectral properties, e.g., significant low energy absorption. Figure 16 shows a plot of the hardness ratio vs the column density that is parameterized by the bremsstrahlung temperature. We adopted two values for the column density for those sources with too few counts for spectral fits: foreground and background objects, 1.55×10^{20} cm^{-2}, and member objects, 5×10^{20} cm^{-2}. This is clearly a crude, but reasonable, approach for estimating the spectral properties of a given source, given the poor statistics for the weaker sources. For those sources for which spectral fits could be carried out, we used the fitted value of the column density. The sources 11, 17, and 19 all appear in Fig. 16 at the extreme right-hand side at the adopted column density of $N_H=1.55\times10^{20}$ cm^{-2}. Clearly, the column density must be higher; the temperature to which *ROSAT* is sensitive is ~1 keV which is excluded by the value of the hardness ratio. These three sources should therefore slide upwards in the plot to fall within the cloud of points at high N_H. As a result, these sources are candidates to be members of NGC 55.

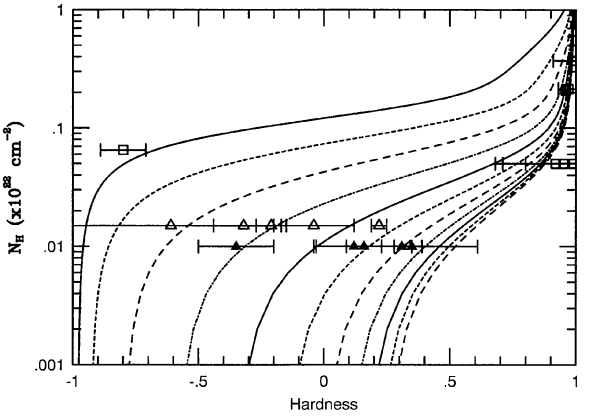

FIG. 16. Hardness ratio plot: the curves parameterize the bremsstrahlung temperature starting at 0.1 keV (top solid line) and progressing in units of 0.2 in log(kT) to 10 keV (bottom dashed line). The data points are the sources from Table 3 (except for sources 2, 4, 6, 18, and 21, for which the error bars were sufficiently large to disrupt the plot). Those sources for which spectral fits exist have been plotted at the best-fit value of N_H. For the weaker sources, the value of N_H has been adopted as follows: likely foreground objects, 0.5×10^{20} cm^{-2} (open triangles); likely members of NGC 55, 1×10^{20} cm^{-2} (squares); likely background objects, 5×10^{20} cm^{-2} (filled triangles).

Figure 17 shows the integrated luminosity distribution of NGC 55 in comparison with the *Einstein* study of M33 (Trinchieri *et al.* 1988). The NGC 55 distribution was constructed by assuming that all of the sources marked "M" or "M?" in Table 3 are, in fact, members of NGC 55. (The reader should consult the appendix and Sec. *3.2* for comments on the membership of the individual sources.) The number distributions for the two galaxies rise in parallel. NGC 55 has fewer numbers of detected sources per luminosity bin because it is nearly edge-on (instead of nearly face-on as is M33) and because it is a galaxy with about 60% of the mass of M33 (Tully 1988). The high inclination will likely hide some sources from *ROSAT* behind a large column depth. With less mass, there will be, on average, fewer massive X-ray binaries formed. Both of these conditions are reflected in the number distribution.

5.2 Diffuse X-ray Emission in NGC 55

If we interpret the diffuse X-ray emission as arising from a hot component of the interstellar medium of NGC 55, we

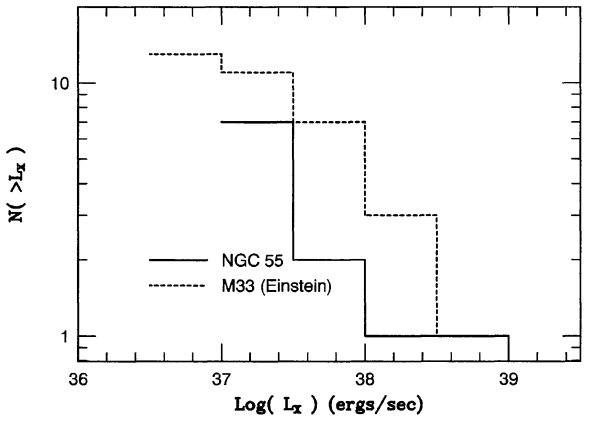

FIG. 17. Integrated number distribution of the point sources believed to belong to NGC 55. For comparison, the number distribution of the *Einstein* data of M33 is used.

may compare it with the detected hot components of other galaxies. Table 5 lists the results of the comparison in which the luminosity of each galaxy's hot diffuse component is listed, as well as the total mass in the galaxy and the ratio of L_X to the total mass. The latter ratio attempts to define a measure of the diffuse emission that is independent of the size of a given galaxy. With this measure, NGC 55 appears to be similar to the edge-on galaxy NGC 891. The fitted temperature of the NGC 55 diffuse emission is about a factor of 3 higher than the temperature of the NGC 891 emission (Bregman & Pildis 1994), but it is similar to the temperature of the hot component of the LMC (e.g., Wang *et al.* 1991). Recall, though, that point sources falling below the 5σ detection threshold could contribute to the diffuse emission; hence, the 1 keV temperature should be considered an upper limit. Statistics are insufficient at this time for any trends in the Table 5 entries to be revealed.

An alternative explanation for the "diffuse" emission is that it represents the summed emission of unresolved point sources. Typical point sources could include supernova remnants, cataclysmic variables, active stars, and X-ray binaries. For example, we can follow the discussion of the discrete source contributions to the X-ray luminosity of a galaxy by Primini *et al.* (1993). Cataclysmic variables, emitting at a typical luminosity of $\sim 10^{30-32}$ ergs s^{-1} (Córdova 1995), fail by at least two orders of magnitude to account for the emission. So, too, do the contributions of active stars which emit at $\sim 10^{31}$ ergs s^{-1}. Supernova remnants ($L_X \sim 10^{36}$ ergs s^{-1}; hereafter SNRs) may account for the emission if there are approximately 100 in the galaxy. But because the galaxy is edge-on, the SNRs must not be absorbed, must emit most of their energy above 0.5 keV, must be preferentially distributed on the near side of the galaxy, or the total number of SNRs must be higher (if they are absorbed). These criteria argue against such an explanation. If the SNRs are preferentially young, however, then the above numbers can be relaxed somewhat because the median L_X will be higher. "Odd" supernovae or SNRs such as SN1978K (Schlegel *et al.* 1996; Ryder *et al.* 1993), SN1988Z (Fabian & Terlevich 1996), or SN1986J (Bregman & Pildis 1992), which emit at luminosities of $\sim 10^{39-40}$ ergs s^{-1}, are excluded from consideration.

TABLE 5. Comparison of the X-ray luminosity of the diffuse component.[a]

Galaxy	log L_X	log M_T	log (L_X/M_T)	T_{gas} (keV)	Reference
NGC 55	38.48	9.87	28.61	~1	This paper
LMC	37.72	10.40	27.32	~0.2–0.9	Wang *et al.* 1991
NGC 891	39.64	11.20	28.44	~0.33	Bregman & Pildis 1994
NGC 4631	39.90	10.70	29.20	~0.3	Wang *et al.* 1995
NGC 5194	40.64	10.89	29.74	~0.3	Ehle *et al.* 1995
NGC 5457	40.46	11.20	29.26	~0.3	Snowden & Pietsch 1995 Cui *et al.* 1996
NGC 6946	38.11	10.81	27.30	~0.5	Schlegel 1994

[a]The M_T values, in solar masses, were obtained from Tully (1988) and Allen (1973).

To date, the LMC contains the largest number of SNRs (25) detected in the X-ray band (Mathewson *et al.* 1983). The L_X number distribution is flat (using bins of half-decade width in L_X from 10^{35} to 10^{38} ergs s^{-1}). The mean value is $\sim 2\times 10^{36}$ ergs s^{-1}, but bright remnants can outshine all of the others. Our 5σ detection threshold is $\sim 6\times 10^{36}$ ergs s^{-1}, so many SNRs with a larger luminosity would be present on our detected sources list (Table 3). It is quite possible that one or more of the sources is a remnant, e.g., source 7. We believe that the flat luminosity distribution of SNRs in the LMC, when applied to NGC 55, argues against large numbers of low L_X SNRs. In addition, the low L_X SNRs are likely to be too cool to explain the observed $kT$of the diffuse emission. One possibility that we can not eliminate is the occurrence of a recent episode of star formation that subsequently created a burst of SNRs which expanded into and reheated the ISM of NGC 55.

Finally, we consider X-ray binaries (XRBs) as contributors to the point source population. XRBs basically come in two flavors, the low- ($L_X \sim 10^{36-37}$ ergs s^{-1}) and the high-luminosity systems ($\sim 10^{38}$ ergs s^{-1}) (White *et al.* 1995). About 30–300 low-luminosity systems could account for the emission, a value comparable to that of our Galaxy. A few high-luminosity systems could also explain the detected luminosity. To match the data, the distribution of either flavor should be relatively uniform along the plane of the disk. That statement assumes that the processes that created the distributions of XRBs in NGC 55 are similar to the Galactic processes. The apparent "bubble" appearance of the X-ray contours in NGC 55 argues against the interpretation that point sources comprise the diffuse emission, because one must then find an explanation for the non-uniform distribution (i.e., the asymmetry above and below the plane). Hot diffuse gas more easily fits the non-axisymmetric picture, yet higher spatial resolution observations are necessary to quantify this issue.

The overlay of the X-ray data onto the optical image of NGC 55 (Fig. 13) shows that the gas appears to lie preferentially below the plane of the galaxy in the south-east quadrant. Near the nucleus/bar region, the emission appears more symmetric as one might expect of hot gas expelled from a small region. In addition, the diffuse gas appears excluded

from the western end of the galaxy. The gas appears to be "pinched" just east of the optical center (or, conversely, the gas blooms out to the south in two places and, to the north, near the bar). The "blooming" suggests that, if the link between sites of star formation and the presence of halo gas (e.g., Rand 1996) is substantiated, active star formation is occurring near the bar and in the southeast quadrant. In the 1.5 keV band, gas only appears near the bar. This hotter gas associated with the bar strengthens the case for active star formation because studies of face-on barred spiral galaxies show enhanced star formation at the ends of the bars. Explanations for the power source of the hot diffuse emission may be found in, for example, Wang *et al.* (1995) for NGC 4631 or Bregman & Pildis (1994) for NGC 891, which are edge-on galaxies with detected hot halos. Both studies make use of the input of mechanical energy from stellar winds and supernova shock waves to heat the gas. The discussions of the power sources will not be repeated here because the NGC 55 observations do not add substantially to the physics.

The behavior of the plume suggests an expansion of hot gas out of the plane of the galaxy. This expansion could be a "chimney" (e.g., Norman & Ikeuchi 1989, and references therein) or a "worm" (Heiles 1984) generated by the outgoing wind of an OB association or the shock from a supernova explosion. A recent example of a chimney discovered in our Galaxy is that of Normandeau *et al.* (1996). We noted in Sec. 4 that the contour that defines the X-ray plume is contained within the H I plume. The combination essentially defines the appearance of a chimney: hot gas within cooler walls. We do not claim that this feature is a chimney without evidence that the hot gas is rising out of the plane of the disk. There are too few counts to measure a spectrum, however crudely. The plume's X-ray emission is likely too weak to be detected in the 1.5 keV image because of insufficient exposure. The Galactic and extragalactic 0.25 keV emission are sufficiently strong to overwhelm the plume's 0.25 keV emission. Hummel *et al.* (1986) note that the plume appears to be connected with a bubble that lies on the north side of the galaxy. We note for the reader that no features in the H I map of Braun (1995) appear to correlate with features in the PSPC data because his data are not sufficiently sensitive. The lowest contour of the Braun data lies at 1×10^{20} cm^{-2}, while in the Hummel *et al.* data, the lowest contour lies at least a factor of 2 or more below that value.

The size of the plume, estimated in Sec. 4, corresponds closely with the sizes estimated for chimneys based upon hydrodynamical modelling (cf. Norman & Ikeuchi 1989). The luminosity of the plume can be estimated from the contour at $\sim1.5\times10^{-4}$ count s^{-1} arcmin^{-2} (the outermost but one). If we assume the contour's surface density applies to the entire plume, and integrate it across the plume, we obtain an approximate lower limit to the luminosity of 10^{36} ergs s^{-1}. We can estimate the number density n_e from

$$L_X = n_e^2 V \Lambda_R(T),$$

where V is the volume of the plume and $\Lambda(T)$ is the cooling function $\sim10^{-23}$ ergs cm^3 s^{-1} for the temperature range of 10^{6-7} K (Wang *et al.* 1989). We calculate a number density n_e of $\sim3.5\times10^{-3}$ cm^{-3}, which is a typical density for the hot component of the Galactic interstellar medium (e.g., Dettmar 1992) or a chimney (e.g., Norman & Ikeuchi 1989). We note that the plume appears in the H I data of Hummel *et al.* (1986) at a heliocentric radial velocity of 152 km s^{-1}; the plume is not visible ±2 channels around that value (channel width=21 km s^{-1}). We infer that the radial velocity of the gas is ~30 km s^{-1} since the systemic velocity is $\sim118\pm4$ km s^{-1} (PCW91). If we assume that the plume has been expanding outward at that velocity, then the time to travel the length of the plume, ~1.4 kpc, is $\sim4-5\times10^7$ yr. A comparable time can be estimated from the total X-ray luminosity (Norman & Ikeuchi 1989).

6. SUMMARY

We have studied the nearly edge-on galaxy NGC 55 using data obtained with the *ROSAT* PSPC. We identify a number of sources that are likely to be gravitationally bound to the galaxy of which one of these sources appears to be a supersoft source. We are endeavoring to obtain optical observations to identify the source. Diffuse emission is detected in the 0.75 and 1.5 keV bands. The 0.75 keV image shows a hot plume that aligns with a plume present in the H I maps made at the VLA (PCW91). The combination of X-ray and radio plumes suggests a chimney at that location. We estimated a few basic parameters of the chimney, all of which agree with models and Galactic observations of similar structures.

A long, high spatial resolution observation is necessary to decide whether the "diffuse" emission arises from unresolved point sources or a hot component. A follow-up observation that goes deeper and has a higher spatial resolution will also be invaluable for probing the plume. It is quite possible that an *HRI* observation will itself be insufficient because of the intrinsically higher background of the *HRI* relative to the detection level of the diffuse emission. The ultimate test for the forseeable future will be an observation using the *AXAF* High Resolution Camera (Murray *et al.* 1987).

We thank the referee for several suggestions which improved the presentation of the material in this paper.

REFERENCES

Allen, C. W. 1973, Astrophysical Quantities (Athlone, University of London)
Barber, C. R., Roberts, T. P., & Warwick, R. S. 1996, MNRAS, 282, 157
Boller, Th., Brandt, W., & Fink, H. 1996, A&A305, 53
Braun, R. 1995, A&AS, 114, 409
Bregman, J. N., & Pildis, R. A. 1994, ApJ, 420, 570
Bregman, J. N., & Pildis, R. A. 1992, ApJ, 398, L107
Cordova, F. 1995, in X-ray Binaries, edited by W. Lewin (Cambridge University Press, Cambridge)
Cui, W., Sanders, W., McCammon, D., Snowden, S., & Womble, D. 1996, ApJ, 468, 102
Dettmar, R.-J. 1992, Fundam. Cosm. Phys., 15, 143

deVaucouleurs, G., *et al.* 1991, Third Reference Catalogue of Bright Galaxies (Springer, Berlin, Heidelberg, New York)
Ehle, M., Pietsch, W., & Beck, R. 1995, A&A, 295, 289
Fabbiano, G. 1989, ARA&A, 27, 87
Fabian, A., & Terlevich, R. 1996, MNRAS, 280, L5
Hasinger, G., Schmidt, M., & Trümper, J. 1991, A&A, 246, L2
Heiles, C. 1994, ApJS, 55, 585
Hoopes, C., Walterbos, R., & Greenawalt, B. 1996, AJ, 112, 1429
Hughes, J. P., *et al.* 1995, ApJ, 444, L81
Hummel, E., Dettmar, R.-J., & Wielebinski, R. 1986, A&A, 166, 97
Liller, W., & Alcaino, G. 1983, ApJ, L264, 53
Mathewson, D., Ford, V., Dopita, M., Tuohy, I., Long, K., & Helfand, D. 1983, ApJS, 51, 345
Murray, S. S., *et al.* 1987, Astro. Lett. Comm., 26, 117
Mushotzky, R., Pounds, K., & Done, C. 1993, ARA&A, 31, 717
Norman, C., & Ikeuchi, S. 1989, ApJ, 345, 372
Normandeau, M., Taylor, A., & Dewdney, P. 1996, Nature 380, 687
Pfeffermann, E., *et al.* 1987, Proc. SPIE, 733, 519
Primini, F., Forman, W., & Jones, C. 1993, ApJ, 410, 615
Pritchett, C. J., Richer, H. B., Schode, D., Crabtree, D., & Yee, H. K. C. 1987, ApJ, 323, 79
Puche, D., Carignan, C., & Wainscoat, R. J. 1991, AJ, 101, 447
Rand, R. J. 1996, ApJ, 462, 712
Rice, W. 1993, AJ, 105, 67
Romero-Colmenero, E., Branduardi-Raymont, G., Carrera, F. J., Jones, L. R., Mason, K. O., McHardy, I. M., & Mittaz, J. P. D. 1996, MNRAS (in press)
Rush, B., Malkan, M., Fink, H., & Voges, W. 1996, ApJ, 471, 190
Ryder, S., Staveley-Smith, L., Dopita, M., Petre, R., Colbert, E., Malin, D., & Schlegel, E. M. 1993, ApJ, 416, 167
Sambruna, R., *et al.* 1994, in The Soft X-ray Cosmos, edited by E. Schlegel and R. Petre (American Institute of Physics, New York), p. 415
Schlegel, E. M. 1994,ApJ, 434, 523
Schlegel, E. M., Petre, R., & Colbert, E. J. M. 1996, ApJ, 456, 187
Singh, K. P., Barrett, P., White, N. E., Giommi, P., & Angelini, L. 1995, ApJ, 455, 456
Singh, K. P., Westergaard, N. J., Schnopper, H. W., & Helfand, D. J. 1987, ApJ, 322, 80
Snowden, S. 1995, Cookbook for Analyzing *ROSAT* Observations of Extended Objects and Diffuse Emission, US *ROSAT* Science Data Center (NASA-GSFC, Greenbelt) (available by anonymous FTP)
Snowden, S., *et al.* 1996, IAU Circ. 6419
Snowden, S., *et al.* 1995, ApJ, 454, 643
Snowden, S., McCammon, D., Burrows, D., & Mendenhall, J. 1994, ApJ, 424, 714
Snowden, S., & Pietsch, W. 1995, ApJ, 452, 627
Stark, A., *et al.* 1992, ApJS, 79, 77
Trinchieri, G., Fabbiano, G., & Peres, G. 1988, ApJ, 325, 531
Tully, R. B. 1988, Nearby Galaxies Catalog (Cambridge University Press, Cambridge)
Voges, W., *et al.* 1996, IAU Circ. 6420
Wang, Q. D., Hamilton, T., Helfand, D., & Wu, X. 1991, ApJ, 374, 475
Wang, Q. D., Hamilton, Q. D. & Helfand, D. 1989, Nature, 341, 309
Wang, Q. D., Walterbos, R. A. M., Steakley, M. F., Norman, C. A., & Braun, R. 1995, ApJ, 439, 176
White, N., Nagase, F., & Parmar, A. 1995, in X-ray Binaries, edited by W. Lewin (Cambridge University Press, Cambridge), p. 1